Hindawi Publishing Corporation
Advances in Condensed Matter Physics
Volume 2014, Article ID 968349, 7 pages
http://dx.doi.org/10.1155/2014/968349

Research Article

Electrical and Dielectric Characterization of $Bi_{12}GeO_{20}$ Prepared by Modified Pechini Method

C. G. P. Moraes,[1] F. A. A. Jesus,[2] and Z. S. Macedo[1]

[1] *Physics Department, Federal University of Sergipe, 49100-000 São Cristóvão, SE, Brazil*
[2] *State University of Santa Cruz, 45662-900 Ilhéus, BA, Brazil*

Correspondence should be addressed to Z. S. Macedo; zelia.macedo@gmail.com

Received 7 April 2014; Accepted 30 June 2014; Published 15 July 2014

Academic Editor: Rosa Lukaszew

Bismuth germanate ($Bi_{12}GeO_{20}$) ceramics were produced using modified Pechini route, and the synthesis parameters, crystalline phases, microstructure, and sintering conditions were investigated. $Bi_{12}GeO_{20}$ powders with submicrometric particle sizes were investigated for calcination temperatures from 400 to 600°C, with soaking times of 1 h and 5 h. Controlling the synthesis parameters, dense ceramics with two different grain sizes of $3.4 \pm 0.5\,\mu$m and $5.7 \pm 0.8\,\mu$m could be produced after sintering at 750°C/1 h. The electric and dielectric properties of these ceramics were determined by impedance spectroscopy (IS). From the results, it was concluded that the dielectric permittivity measured at high frequencies is insensitive to the grain size, while the AC dark conductivity presents a noticeable dependency on this feature. This behaviour was discussed on the basis of a Maxwell-Wagner interfacial relaxation, whose intensity depends directly on the volume fraction of grain boundaries in the sample.

1. Introduction

Bismuth germanate ($Bi_{12}GeO_{20}$) belongs to a class of materials known as sillenites with general formula $Bi_{12}MO_{20}$, where M represents a tetravalent ion or a combination of ions yielding average charge 4+ [1, 2]. Sillenites crystallize in the cubic system (space group I23) and usually present photorefractive and electrooptical properties [3–5] that make them useful as recording media, optical switching, and sensors, among others [6–9]. For optical applications, transparency and crystalline coherence are required, so the devices employ single crystals. Nevertheless, for UV and high energy sensors, transparency is not a requirement since either the electrical conductivity or the dielectric permittivity can be used to monitor radiation doses. On the other hand, a good control of grain size and purity of the material can determine the sensitivity and good resolution of such devices.

Some synthesis routes have been proposed to obtain $Bi_{12}GeO_{20}$ single crystals and ceramics [10–14], but to our knowledge Pechini route has not been reported up to now for the production of $Bi_{12}GeO_{20}$ or any other sillenites. Pechini process has emerged as a powerful method to obtain nanocrystalline powders in several compositions. This synthesis route allows the formation of a polymeric net (resin) containing the metallic ions homogeneously distributed. The resin formation occurs in three steps: metallic chelate formation, ester formation, and polyesterification [14–16]. The original Pechini method mixes metallic citrates first and then adds polyhydroxy alcohols [14]. The main advantage of this method is the good control of the stoichiometry, high purity, easy dopant incorporation, and formation of nanometric or submicrometric particles with controlled particle size.

In a previous paper, the mechanisms of dark conductivity and dielectric relaxation of $Bi_{12}GeO_{20}$ ceramics produced by solid state reaction were reported [9]. It was observed that high resistivity of the grain interfaces leads to Maxwell-Wagner polarization of the grain boundaries due to local charge rearrangement [9]. In this work impedance spectroscopy (IS) was utilized to determine the AC conductivity and dielectric permittivity of the bismuth germanate ceramics obtained by modified Pechini method, comparing the obtained parameters with those reported in the literature and investigating the influence of the grain size on these properties [9, 17–20]. Additionally, the synthesis parameters

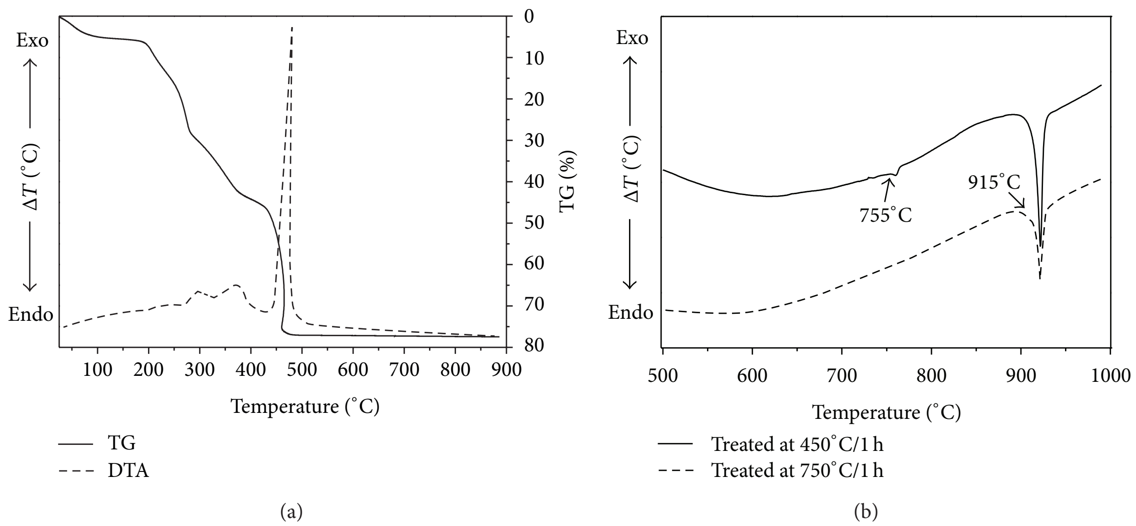

Figure 1: (a) Simultaneous DTA/TG curves of the resin dried at 100°C/24 h. (b) DTA curves obtained after thermal treatments at 450°C/1 h and 750°C/1 h.

and structural and microstructure characterization of the powders and dense ceramics are presented and discussed.

2. Experimental

$Bi_{12}GeO_{20}$ powders were synthesized by the polymeric precursor method using bismuth oxide (Bi_2O_3; VETEC, 3N) and germanium oxide (GeO_2; Alfa Aesar, 5N). Firstly, Ge and Bi solutions were prepared, respectively, by dissolving GeO_2 in distilled water at 90°C in a concentration of 0.005 g mL^{-1} [16] and Bi_2O_3 in nitric acid (diluted with distilled water) in a concentration of 0.120 g mL^{-1}. These cationic solutions were separately mixed with citric acid (CA; VETEC, 3N) previously dissolved in distilled water (0.1 g mL^{-1}) at a molar ratio of 1 : 3 (Cation : CA) [16]. Ethylenediamine (ED; VETEC, 3N) was slowly added to adjust pH of bismuth citrate at 9.0, which is essential to the solution stability. To activate the polymerization reaction, each citrate solution was kept at 90°C and separately mixed with ethylene glycol (EG; $C_2H_6O_2$; VETEC, 3N), at the molar ratio of 6 : 4 (Cation : EG). After that, Ge solution was slowly added to Bi solution under stirring, keeping pH = 9.0. After the complete homogenization, this material was dried at 100°C for 24 h, resulting in a yellowish polymeric resin.

The dried resin was characterized by thermogravimetry (TG) and differential thermal analysis (DTA) using a simultaneous DTA/TG (SDT 2960; TA Instruments). In these analyses the samples were kept under synthetic air flow (120 mL min^{-1}) and heated from 25 up to 1000°C with heating rate of 10°C min^{-1}. The results from DTA/TG have guided the calcination tests of this resin carried out in a muffle-type furnace, using different temperatures and soaking times, as it will be discussed in the next section.

After the calcination, the $Bi_{12}GeO_{20}$ powder was milled again for 20 min, mixed to a binder solution of polyvinyl alcohol, conformed by uniaxial pressing under 15 MPa in disks 4 mm in diameter and 2 mm thick for sintering and 8 mm thick for dilatometric analyses. These dilatometric studies were performed in a NETZSCH-402PC dilatometer, with heating rate of 10°C/min and air flux of 120 mL/min. The results obtained from the dilatometric tests guided the sintering, which was performed in a muffle-type furnace. A batch of three samples was made at each sintering condition.

The relative density of the sintered ceramics was determined by the fluid displacement (Archimedes) method, using distilled water [21, 22]. The crystalline phases of the powder and sintered ceramics were inspected by X-ray diffraction (XRD; Rigaku RINT 2000/PC), in continuous scanning mode using Cu K_α radiation, in the 2θ range between 10° and 80°. The particle size of the calcined powders was obtained from the analysis of 5 SEM images (JEOL 6510LV and PHILIPS XL 30 FEG). The average grain size of the sintered ceramics was determined from the analysis of at least 3 SEM images, using the linear intercept technique [23], in which the grain shape was assumed to be spherical.

For the impedance spectroscopy measurements, the opposite faces of the cylindrical samples were polished with silicon carbide, cleaned with acetone in ultrasonic bath for 15 minutes, and dried at 100°C. Electric contact was made by applying Pt paste on the parallel faces of the pellets and firing them at 700°C for 30 minutes. The measurements were performed in a two-electrode configuration cell, in the frequency range from 10 Hz to 30 kHz, using a Solartron Impedance/Gain-Phase Analyzer SL 1260. The applied potential was 2 V and all the measurements were taken isothermally, with a tolerance of 1% in temperature.

3. Results and Discussion

The thermal behavior of the polymeric resin is presented in Figure 1(a) and was investigated in order to identify the best calcination temperature to produce $Bi_{12}GeO_{20}$.

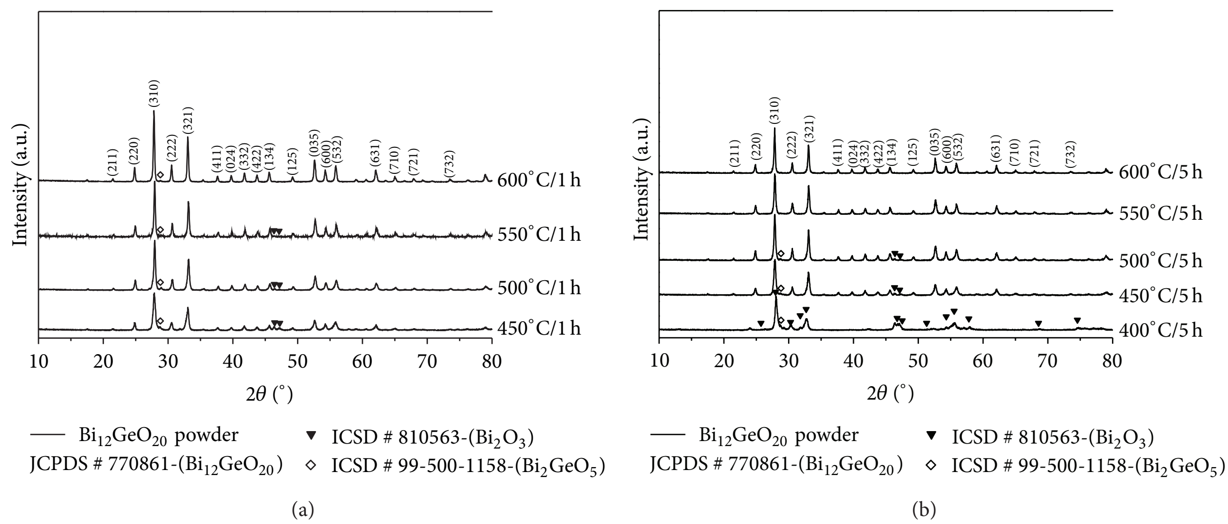

Figure 2: X-ray diffraction patterns of the $Bi_{12}GeO_{20}$ powders calcined at temperatures from 400 to 600°C with calcination times of 1 h or 5 h.

The main thermal event in DTA curve is an exothermic peak observed between 420 and 480°C, accompanied by a mass loss of 32%. This event can be associated to combustion reactions, organic decomposition, and subsequent formation of crystalline phase. Three exothermic events with a total mass loss of ~45% can be observed below 400°C and are possibly related to dehydration, oxidation reactions, and NO_x elimination. These results suggest that $Bi_{12}GeO_{20}$ crystallizes at temperatures near 450°C, which is 230°C below the lowest value reported in literature [9] for the production of this material. Figure 1(b) presents the DTA curves obtained after thermal treatment at 450°C and 750°C, respectively. According to the equilibrium phase diagram of the binary mixture Bi_2O_3/GeO_2, $Bi_{12}GeO_{20}$ is the most stable phase in the region with GeO_2 concentrations from 32 to 1 mol% [7, 24]. However, according to these authors, the metastable phase Bi_2GeO_5, as well as the Bi_2O_3 component, can also be found between 437 and 792°C [24]. As one can see in Figure 1(b), the powder calcined 450°C undergoes a thermal event at 755°C, while the sample treated at 750°C presents only an endothermic peak with onset at 910°C, which corresponds to the melting point of $Bi_{12}GeO_{20}$. To reach a deeper understanding of the reactions occurring during the synthesis, a systematic study of the calcined powders was carried out using XRD technique.

Figure 2 presents XRD patterns of the powders calcined at different temperatures during 1 h or 5 h, as indicated in each curve. The presence of major phase $Bi_{12}GeO_{20}$ can be observed for all the samples analysed. Minor phases β-Bi_2O_3 and Bi_2GeO_5 were also observed for the samples calcined at $T \leq 600$°C for 1 h or $T \leq 500$°C for 5 h. Comparing these results with the DTA curves presented in Figure 1(b), it can be concluded that the endothermic event at 755°C is related to the reaction between β-Bi_2O_3 and Bi_2GeO_5 to form $Bi_{12}GeO_{20}$. This reaction occurred at lower temperatures when longer soaking times were employed, so, for the samples calcined during 1 h or 5 h, single phase $Bi_{12}GeO_{20}$ was obtained at 600°C or 550°C, respectively.

Figure 3 presents SEM images of the powders calcined for 1 h at 450°C and 600°C. As a general feature, it can be observed that the samples have well-dispersed submicrometric particles, with sizes of about 200 (±100) nm for the sample produced at 450°C and 500 (±100) nm when $T = 600$°C was used for the synthesis. It can also be noticed that some plate-like structures are present in the sample produced at lower temperatures (see Figure 3(c)). These particles are possibly β-Bi_2O_3, also detected by XRD measurements (see Figure 2). On the other hand, the samples produced at 600°C (see Figure 3(e)) presented only rounded particles, corresponding to the single phase $Bi_{12}GeO_{20}$ observed in the XRD patterns.

Smaller particles can favour the packing process during the sintering of the ceramic bodies. Figure 4 presents the measured shrinkage and its derivative as a function of the sintering temperature for compacts prepared with the powders produced at 450 or 600°C. The maximum shrinkage rate was determined at 723°C and 756°C, respectively, for the samples synthesized at 450°C (Figure 4(a)) and 600°C (Figure 4(b)). Based on these values, the sintering tests were carried out at 750°C, with soaking time of 1 h. Hereafter, the sintered ceramics produced using the powders calcined at 450°C and 600°C will be called C450 and C600, respectively.

Figure 5 presents the XRD patterns of the samples C450 and C600, confirming that single phase $Bi_{12}GeO_{20}$ was obtained for both the sintered ceramics. Figure 6 presents SEM images of these sintered samples, where the grains at the final stage of sintering can be observed. The density of the sintered samples was the same ($8.3 \pm 0.1\,g/cm^3$) for both samples, but a noticeable difference between the average grain sizes was registered. The sample C450 presented average grain size $3.4 \pm 0.5\,\mu m$, while the value $5.7 \pm 0.8\,\mu m$ was determined for the sample C600. It is well known that the average size, as well as the properties of the material, may depend on

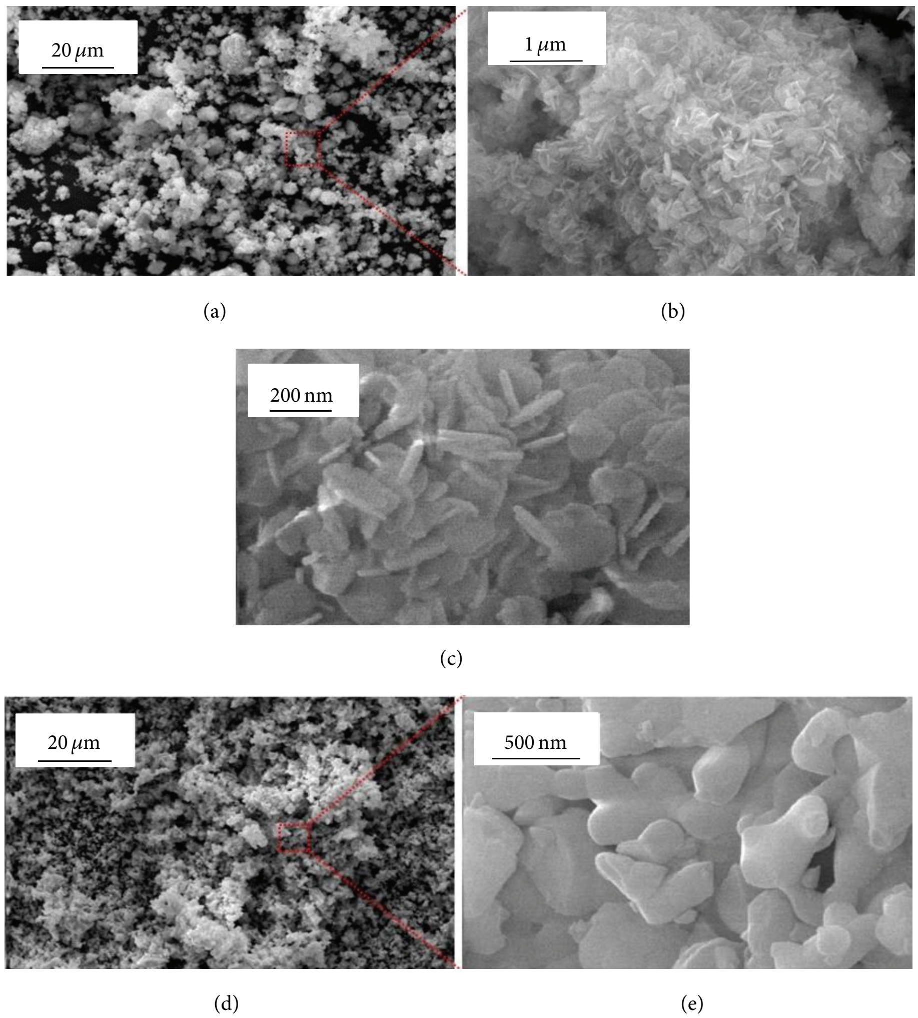

FIGURE 3: SEM images of the powders calcined at (a), (b), and (c) 450°C/1 h; (d) and (e) 600°C/1 h.

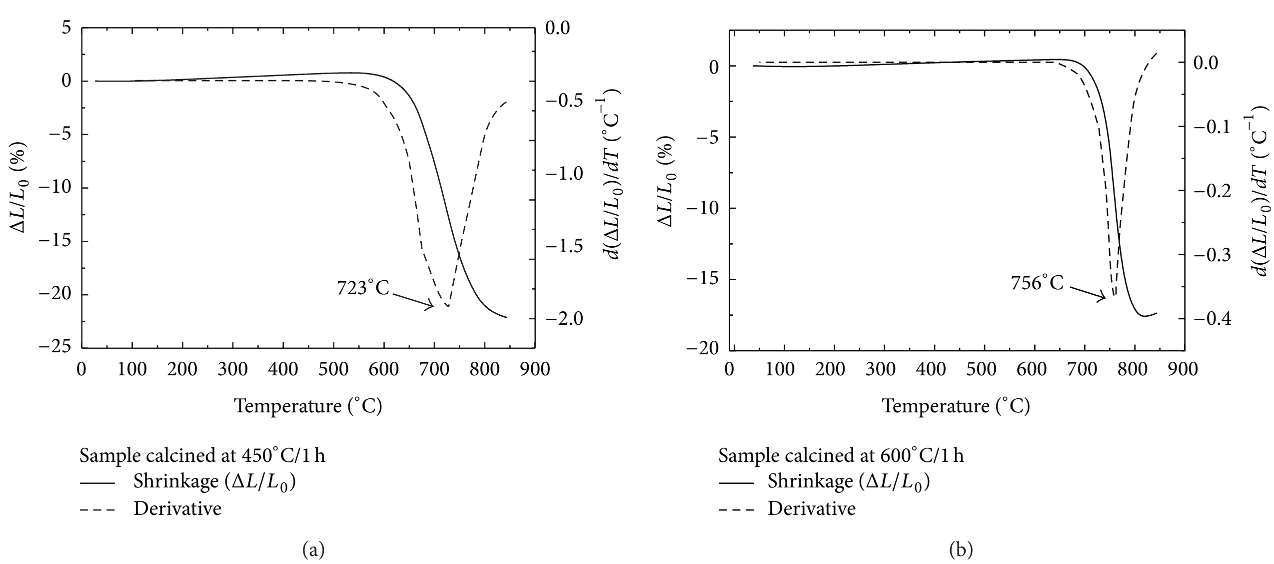

FIGURE 4: Dilatometric analysis of the samples calcined at (a) 450°C/1 h and (b) 600°C/1 h. Closed symbols represent the shrinkage and open symbols represent the shrinkage rate.

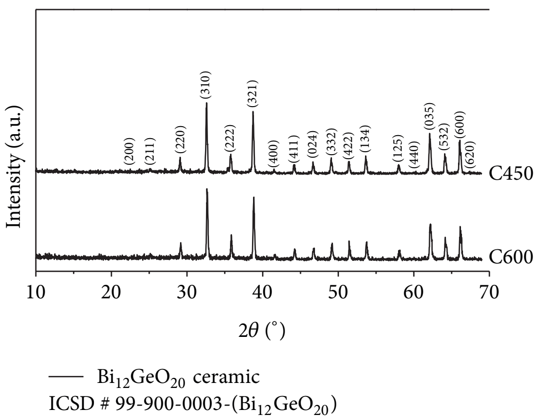

Figure 5: X-ray diffraction patterns of the samples C450 (calcined at 450°C/1 h and sintered at 750°C/1 h) and C600 (calcined at 600°C/1 h and sintered at 750°C/1 h).

the preparation method and synthesis conditions [25–27]. Impedance spectroscopy (IS) was employed to determine the AC conductivity and dielectric permittivity of the $Bi_{12}GeO_{20}$ ceramics, in order to investigate the influence of the grain size on these properties.

The AC conductivity is the real part of the complex admittance and can be obtained from the impedance data using (1). In this equation, d and A are the thickness of the sample and the area of the electrodes, respectively:

$$\sigma(\omega) = \mathrm{Re}\left[\left(Z^*\right)^{-1}\right]\frac{d}{A}. \tag{1}$$

Figure 7 presents the AC dark conductivity as function of the frequency for samples C450 and C600. It can be observed that both curves present the same profile, but the sample C450 has higher conductivity. The conductivity measured at 250°C and low frequencies were about 5×10^{-9} S/cm for sample C450 and 4×10^{-10} S/cm for sample C600. These values are comparable with some values reported in [9, 17, 18], although the experimental conditions were not exactly the same. The higher conductivity was observed for the ceramic with smaller grains. Considering that the internal conductivity of each grain would be the same for both samples, since they were sintered at the same conditions, the higher conductivity of sample C450 can be attributed to local charge transport in the grain boundaries. In fact, it was already reported that space charge rearrangement occurs at the intergrain region of $Bi_{12}GeO_{20}$ ceramics [9], resulting in Maxwell-Wagner polarization of the grain boundaries. To check this possibility, the dielectric permittivity of the samples was analyzed.

The dielectric permittivity of a material is calculated from the impedance data, using

$$\varepsilon' = \mathrm{Re}\left[\left(i\omega C_0 Z^*\right)^{-1}\right], \tag{2}$$

where C_0 is the empty cell capacitance and ω is the angular frequency $\omega = 2\pi f$. Corrections for the ceramic porosity were made using Maxwell's model [28, 29]. This model considers that, in a ceramic with porosity P, the pores are spheres with $\varepsilon'_p = 1$ embedded in the ceramic matrix with permittivity ε'_m. As a result, the relation between the experimental ε' and the corrected ε'_m is given by

$$\varepsilon' = \varepsilon'_m\left(1 - \frac{3P\left(\varepsilon'_m - 1\right)}{2\varepsilon'_m + 1}\right). \tag{3}$$

Figure 8 presents the dielectric permittivity obtained for the ceramic matrix (ε'_m) using (3) for both samples studied. At low frequencies, the values are strongly dependent on the grain size, with values of 10^3 and 2×10^2 measured at 10 Hz for the samples C450 and C600, respectively. Furthermore, sample C450 presents a dielectric profile with a slight shoulder between 10^2 and 10^3 Hz, indicating interfacial polarization of the grain boundaries [9]. The low frequency dielectric response of ceramics is attributed to grain boundaries [30] and the dispersion of the permittivity values is explained by the movement of charge carriers [31]. In this case, this movement occurs probably in the space charge region at the grain boundaries [32]. At higher frequencies ($f = 30$ kHz), the values presented in Figure 8 are $\varepsilon'_m = 47$ for sample C450 and $\varepsilon'_m = 44$ for sample C600. These values are in good agreement with [9, 17], which have reported $\varepsilon' = 38$ ($f = 5.5$ GHz, $T = 250$°C) and $\varepsilon' = 45$ ($f = 30$ kHz, $T = 250$°C) for $Bi_{12}GeO_{20}$ ceramics produced via solid state route, although no porosity corrections were made in those references. For single crystals, the values reported in literature are $\varepsilon' = 44$ at $f = 1$ kHz and $T = 25$°C [19, 20], which also agree with the values determined in the present work. The low sensitivity of ε'_m to the grain size, when measured at high frequencies, was previously mentioned in [28] and indicates that the polarization processes do not depend on the volume fraction of grains and grain boundaries in the sample.

4. Conclusions

Single phase $Bi_{12}GeO_{20}$ was successfully produced by the modified Pechini method, with calcinations at 600°C/1 h or at 550°C/5 h. For the samples calcined at 450°C/1 h, single phase was obtained after sintering the ceramic bodies. These fabrication conditions are advantageous if compared to the synthesis parameters used for solid state route, which were 850°C in [17] and 680°C/5 h according to [9]. The use of low temperatures allowed the control of the final grain size of the sintered ceramics. Electrical and dielectric characterizations of ceramics with grain sizes of 3.4 ± 0.5 μm and 5.7 ± 0.8 μm were analysed. From the results, it can be concluded that these values are comparable to those ones previously reported for ceramics and single crystals, validating the synthesis method. Additionally, it was observed that the dielectric permittivity measured at high frequencies is insensitive to the grain size, while the AC conductivity presents a noticeable dependency

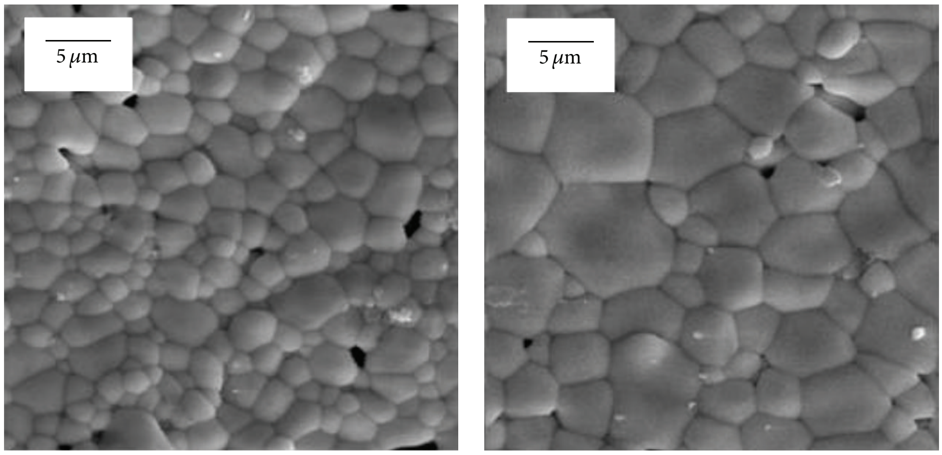

Figure 6: SEM images of the samples C450 (a) and C600 (b).

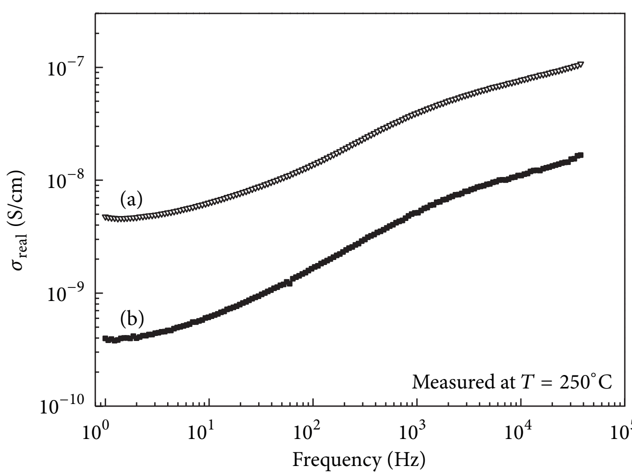

Figure 7: Dark conductivity as function of the frequency of the ceramics sintered at 750°C/1 h, using the powders calcined at (a) 450°C/1 h and (b) 600°C/1 h.

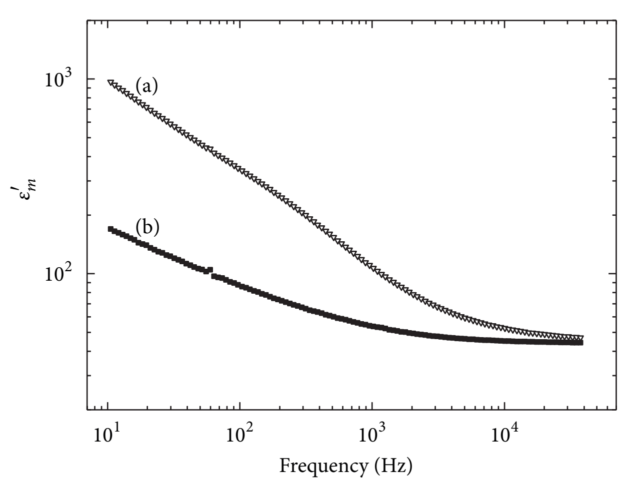

Figure 8: Dielectric permittivity as function of the frequency of the ceramics sintered at 750°C/1 h, using the powders calcined at (a) 450°C/1 h and (b) 600°C/1 h.

on the grain size, probably due to the displacement of charge carriers in the space charge regions.

Conflict of Interests

The authors declare that there is no conflict of interests regarding the publication of this paper.

Acknowledgments

The authors wish to acknowledge CMNano-UFS for the microscopy facilities and the funding agencies CNPq, CAPES, and FAPITEC/SE for the financial support.

References

[1] B. Mihailova, M. Gospodinov, and L. Konstantinov, "Raman spectroscopy study of sillenites. I. Comparison between Bi_{12}(Si,Mn)O_{20} single crystals," *Journal of Physics and Chemistry of Solids*, vol. 60, no. 11, pp. 1821–1827, 1999.

[2] P. Gunter and J. Huignard, *Photorefractive Materials and Their Applications 2: Materials*, vol. 2, Springer, Berlin, Germany, 2007.

[3] P. A. Williams, A. H. Rose, K. S. Lee, D. C. Conrad, G. W. Day, and P. D. Hale, "Optical, thermo-optic, electro-optic, and photoelastic properties of bismuth germanate ($Bi_4Ge_3O_{12}$)," *Applied Optics*, vol. 35, no. 19, pp. 3562–3569, 1996.

[4] J. F. Carvalho, R. W. A. Franco, C. J. Magon, and L. A. O. Nunes, "Vanadium characterization in BTO:V sillenite crystals," *Materials Research*, vol. 2, no. 2, pp. 87–91, 1999.

[5] I. F. Vasconcelos, M. A. Pimenta, and A. S. B. Sombra, "Optical properties of $Bi_{12}SiO_{20}$ (BSO) and $Bi_{12}TiO_{20}$ (BTO) obtained by mechanical alloying," *Journal of Materials Science*, vol. 36, no. 3, pp. 587–592, 2001.

[6] N. Benjelloun, M. Tapiero, J. P. Zielinger, F. Marsaud, and J. C. Launay, "Characterization of deep levels in $Bi_{12}GeO_{20}$ by photoinduced current transient spectroscopy," *Journal of Applied Physics*, vol. 64, no. 8, pp. 4013–4023, 1988.

[7] R. A. Ganeev, A. I. Ryasnyansky, R. I. Tugushev, M. K. Kodirov, and F. R. Akhmedjanov, "Nonlinear optical characteristics of

BSO and BGO photorefractive crystals in visible and infrared ranges," *Optical and Quantum Electronics*, vol. 36, no. 9, pp. 807–818, 2004.

[8] V. M. Skorikov, I. S. Zakharov, V. V. Volkov, and E. A. Spirin, "Transmission and absorption spectra of $Bi_{12}GeO_{20}$, $Bi_{12}SiO_{20}$, and $Bi_{12}TiO_{20}$ single crystals," *Inorganic Materials*, vol. 38, no. 2, pp. 172–178, 2002.

[9] Z. S. MacEdo, C. S. S. Oliveira, and A. C. Hernandes, "Dielectric relaxation mechanism of single crystal and polycrystal bismuth germanate," *Journal of Applied Physics*, vol. 102, no. 3, 2007.

[10] S. Chehab, P. Conflant, M. Drache, J. Boivin, and G. McDonald, "Solid-state reaction pathways of Sillenite-phase formation studied by high-temperature X-ray diffractometry and differential thermal analysis," *Materials Research Bulletin*, vol. 38, no. 5, pp. 875–897, 2003.

[11] V. V. Zyryanov, V. I. Smirnov, and M. I. Ivanovskaya, "Mechanochemical synthesis of crystalline compounds in the Bi_2O_3-GeO_2 system," *Inorganic Materials*, vol. 41, no. 6, pp. 618–626, 2005.

[12] Y. Wang, R. He, M. Yang et al., "Hydrothermal growths, optical features and first-principles calculations of sillenite-type crystals comprising discrete MO_4 tetrahedra," *CrystEngComm*, vol. 14, no. 3, pp. 1063–1068, 2012.

[13] Z. Ž. Lazarević, P. Mihailović, S. Kostić et al., "Determination of magneto-optical quality and refractive index of bismuth germanium oxide single crystals grown by Czochralski technique," *Optical Materials*, vol. 34, no. 11, pp. 1849–1859, 2012.

[14] M. P. Pechini, "Method of preparing lead and alkaline earth titanates and niobates and coating method using the same to form a capacitor," United State Patent Office, no. 3.330.697, 1967.

[15] R. S. Da Silva, M. I. B. Bernardi, and A. C. Hernandes, "Synthesis of non-agglomerated $Ba_{0.77}Ca_{0.23}TiO_3$ nanopowders by a modified polymeric precursor method," *Journal of Sol-Gel Science and Technology*, vol. 42, no. 2, pp. 173–179, 2007.

[16] F. A. A. de Jesus, R. S. D. Silva, and Z. S. MacEdo, "Synthesis of $Bi_4Ge_3O_{12}$ ceramic scintillators by the polymeric precursor method," *Journal of Thermal Analysis and Calorimetry*, vol. 100, no. 2, pp. 537–541, 2010.

[17] M. Valant and D. Suvorov, "Processing and dielectric properties of sillenite compounds $Bi_{12}MO_{20-\delta}$ (M = Si, Ge, Ti, Pb, Mn, $B_{1/2}P_{1/2}$)," *Journal of the American Ceramic Society*, vol. 84, no. 3–12, pp. 2900–2904, 2001.

[18] A. Y. Kudzin, S. N. Plyaka, and G. K. Sokolyanskiĭ, "Effect of vanadium doping on the electrical properties of $Bi_{12}GeO_{20}$ crystals," *Physics of the Solid State*, vol. 42, no. 5, pp. 861–865, 2000.

[19] J. Link, J. Fontanella, and C. G. Andeen, "Temperature variation of the dielectric properties of bismuth germanate and bismuth germanium oxide," *Journal of Applied Physics*, vol. 51, no. 8, pp. 4352–4355, 1980.

[20] K. K. Jain and S. C. Kashyap, "Pressure and temperature dependent dielectric dispersion in $Bi_{12}GeO_{20}$ (100) single crystals," *Bulletin of Materials Science*, vol. 19, no. 3, pp. 533–537, 1996.

[21] ABNT, "NBR-6220—Materiais refratários densos—Determinação da densidade de massa aparente, porosidade aparente, absorção e densidade aparente da parte sólida—Método de ensaio," Associação Brasileira de Normas Técnicas, 1997.

[22] Z. S. Macedo, M. H. Lente, J. A. Eiras, and A. C. Hernandes, "Dielectric and ferroelectric properties of $Bi_4Ti_3O_{12}$ ceramics produced by a laser sintering method," *Journal of Physics Condensed Matter*, vol. 16, no. 16, pp. 2811–2818, 2004.

[23] ASTM, *E112-96—Methods for Determining Average Grain Size*, ASTM, 2004.

[24] V. P. Zhereb and V. M. Skorikov, "Metastable states in bismuth-containing oxide systems," *Inorganic Materials*, vol. 39, supplement 2, pp. S121–S145, 2004.

[25] A. Kumar, R. K. Dwivedi, and O. Parkash, "Low temperature dielectric relaxation in $Ba_{1-x}Bi_xTi_{1-x}Fe_xO_3$ system," *Journal of Materials*, vol. 2013, Article ID 857201, 8 pages, 2013.

[26] B. Behera, E. B. Araújo, R. N. Reis, and J. D. S. Guerra, "AC conductivity and impedance properties of $0.65Pb(Mg_{1/3}Nb_{2/3})O_3$-$0.35PbTiO_3$ ceramics," *Advances in Condensed Matter Physics*, vol. 2009, Article ID 361080, 6 pages, 2009.

[27] V. Pal, R. K. Dwivedi, and O. P. Thakur, "Dielectric and ferroelectric properties of lead-free $1 - z\{(Bi_{1-x}La_x)_{0.5}(Na_{1-y}Li_y)_{0.5}$ $Tio_3\} - zBaTiO_3$ ceramic system," *Advances in Materials Science and Engineering*, vol. 2013, Article ID 125634, 7 pages, 2013.

[28] S. J. Penn, N. M. Alford, A. Templeton et al., "Effect of porosity and grain size on the microwave dielectric properties of sintered alumina," *Journal of the American Ceramic Society*, vol. 80, no. 7, pp. 1885–1888, 1997.

[29] J. C. Maxwell, *A Treatise on Electricity and Magnetism*, vol. 1, Clarendon Press Series, 1873.

[30] J. R. Macdonald and E. Barsoukov, *Impedance Spectroscopy Theory, Experiment, and Applications*, John Wiley & Sons, New York, NY, USA, 2nd edition, 2005.

[31] C. Elissalde and J. Ravez, "Ferroelectric ceramics: defects and dielectric relaxations," *Journal of Materials Chemistry*, vol. 11, no. 8, pp. 1957–1967, 2001.

[32] J. Maier, "Ionic conduction in space charge regions," *Progress in Solid State Chemistry*, vol. 23, no. 3, pp. 171–263, 1995.

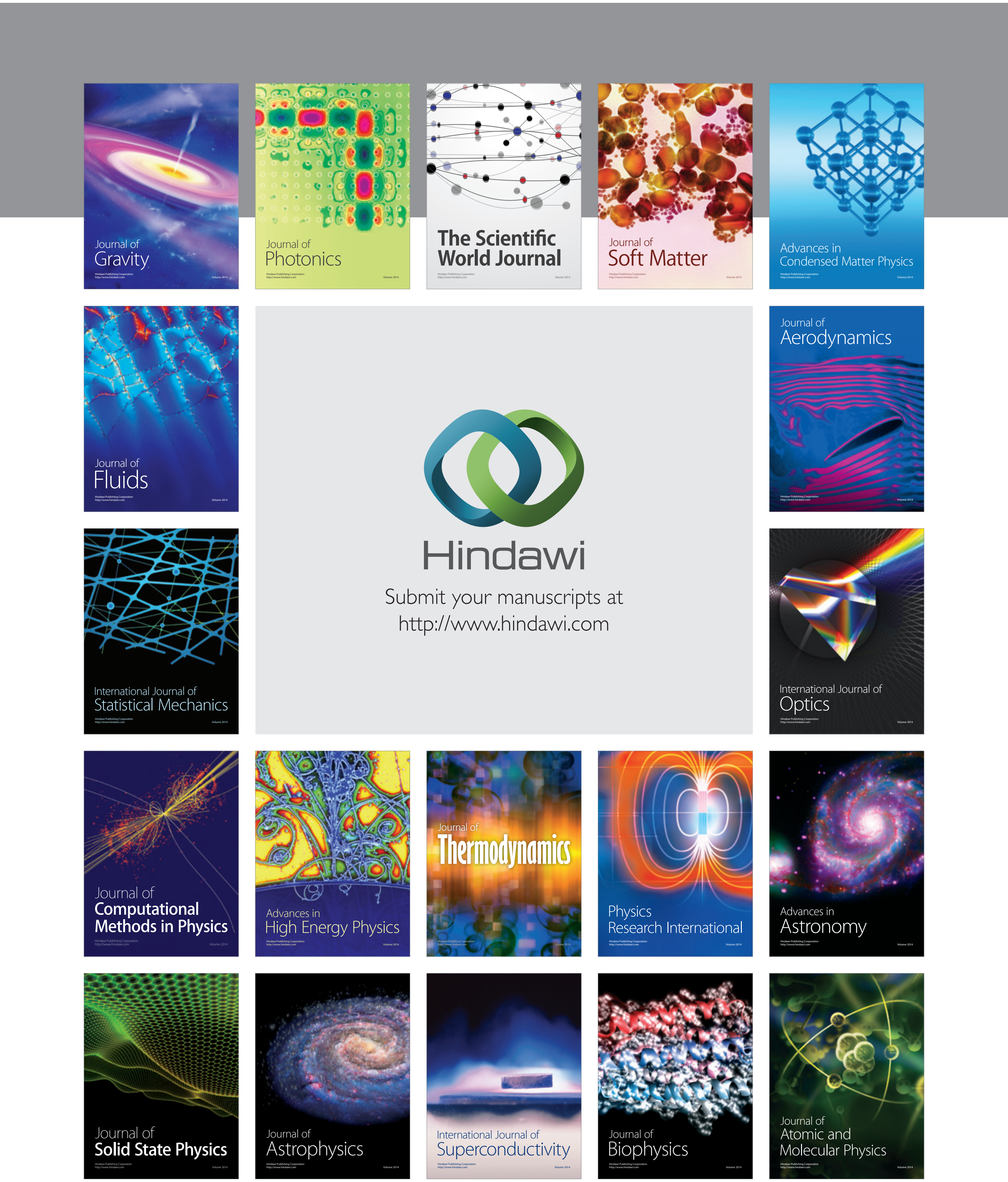
Journal of Gravity
Journal of Photonics
The Scientific World Journal
Journal of Soft Matter
Advances in Condensed Matter Physics
Journal of Fluids
Journal of Aerodynamics
Hindawi
Submit your manuscripts at
http://www.hindawi.com
International Journal of Statistical Mechanics
International Journal of Optics
Journal of Computational Methods in Physics
Advances in High Energy Physics
Journal of Thermodynamics
Physics Research International
Advances in Astronomy
Journal of Solid State Physics
Journal of Astrophysics
International Journal of Superconductivity
Journal of Biophysics
Journal of Atomic and Molecular Physics